Interfacial charge storage mechanisms of composite electrodes based on poly(ortho -phenylenediamine)/carbon nanotubes via advanced electrogravimetry

El Mahdi Halim, Rezan Demir-Cakan, Hubert Perrot, Mama El Rhazi, Ozlem Sel

Interfacial charge storage mechanisms of composite electrodes based on poly(*ortho*-phenylenediamine)/carbon nanotubes *via* advanced electrogravimetry

El Mahdi Halim [†,‡], *Rezan Demir-Cakan* [§,¥], *Hubert Perrot* [†], *Mama El Rhazi* [‡], *Ozlem Sel* [†,*]

[†] Sorbonne Université, CNRS, Laboratoire Interfaces et Systèmes Electrochimiques, LISE, 75005 Paris, France

[‡] University of Hassan II of Casablanca, Faculty of Sciences and Technology, Laboratory of Materials, Membranes and Environment-BP 146, 20650 Mohammedia, Morocco

[§] Institute of Nanotechnology, Gebze Technical University, 41400 Gebze, Kocaeli, Turkey

[¥] Department of Chemical Engineering, Gebze Technical University, 41400 Gebze, Kocaeli, Turkey

* Corresponding author: ozlem.sel@sorbonne-universite.fr

ABSTRACT:

To reach a deeper understanding of the charge storage mechanisms of electrode materials is one of the challenges towards improving its energy storage performance. Herein, we investigate the interfacial ion exchange of a composite electrode made of carbon nanotube/poly(*ortho*-phenylenediamine) (CNT/P*o*PD) in a 1M NaCl aqueous electrolyte *via* advanced electrogravimetric analyses based on electrochemical quartz crystal microbalance (EQCM). Classical EQCM at different scan rates of the potential revealed the complex electrogravimetric behavior, likely due to multi-species participation at different temporal scales. Thereafter, in order to better understand the behavior of each species (ion, counter ion, co-ions) in the charge compensation mechanism, the electrogravimetric impedance spectroscopy analysis (also called *ac*-electrogravimetry) was pursued. *Ac*-electrogravimetry revealed the role of each species where Na^+ cations, Cl^- anions as well as protons participate in the charge compensation mechanism of the CNT/P*o*PD composite, with different kinetics and proportions. The water molecules, with opposite flux direction with the cations, are also detected suggesting their exclusion during cationic species transfer. Having analyzed *ac*-electrogravimetry responses in depth, the positive synergistic interaction between the CNT and the P*o*PD is highlighted revealing the creation of other electro-active sites in the nanocomposite electrode for ion exchange.

KEYWORDS: Interfacial ion dynamics, electrochemical quartz crystal microbalance, *ac*-electrogravimetry, carbon nanotubes, poly(*ortho*-phenylenediamine), nanocomposite

1. INTRODUCTION

The growth in the use of electronic devices such as laptops, phones, and tablets, in addition to the trend towards using electric vehicles have led to a strong and rapid demand for energy and high-performance energy storage devices.[1,2] Supercapacitors and batteries are electrochemical energy storage systems, which play a significant role in the electronic and transport areas.[3] Their efficiency relies strongly on the properties of the electrode materials, especially, their morphology, surface area, and porosity.[4,5]

Electrochemical double layer capacitors, also called supercapacitors, are promising energy storage systems, which present a long-life cycle and high-power density, and store energy *via* adsorption/desorption process of ions at the electrode/electrolyte interface. Carbon materials such as porous carbon, carbon nanotubes (CNTs) and graphene have been extensively studied as electrode material for supercapacitors.[6,7] They can store energy through a reversible electrostatic process, in which the electrolyte ions are accumulated onto the surface. However, in order to achieve a maximum specific capacitance, the correlation between the pore size of the electrode material and the ions size should be optimized.[8–10] Therefore, understanding the charge storage properties of electrode material in the nanometric scale is a very important factor to consider in enhancing the performance of supercapacitors.

A substantial research effort has been conducted to understand the charge storage mechanisms of the electrode materials using electrogravimetric methods. Ye *et al*.[11] used electrochemical quartz crysal microbalance (EQCM) to investigate the charge storage process of Single-Layer Graphene (SLG) in neat ionic liquid. The results show that the double-layer charging of SLG is dominated by desorption of positively charged ions/species and reorganization of them. The charge storage properties of SWCNT have been as well studied by EQCM. Barisci *et al*.[12] reported that the ions transfer onto SWCNT film is complex, since the formation of double-

layer depends on multiple parameters, for instance the nature of electrolyte ions, and the electrogravimetric behavior at positive potentials is different to that occurring at negative potentials. Thus, in addition to the classical EQCM studies that provides a global response of the charge compensation process, Escobar-Teran *et al*.[13] employed *ac*-electrogravimetry as an alternative characterization method, to better understand this global EQCM response and to deconvolute the electrogravimetric behavior of SWCNT-based electrode. It was found that in aqueous NaCl electrolyte, while hydrated sodium ion and proton participate at cathodic potentials, chloride ion and water molecules participate at anodic potentials during the electro-adsorption process at SWCNT electrode, with different kinetics. These results showed a good correlation with EQCM response which confirm the conclusions drawn.

Ac-electrogravimetric method is based on coupling quartz crystal microbalance with electrochemical impedance spectroscopy. It can provide an access to relevant information occurring at the electrode/electrolyte interface (EEI): (i) identification of species involved in the electrochemical processes (with their flux directions at the EEI), (ii) separation of their nature (charged and non-charged), (iii) determination of their kinetics, and (iv) variation of their relative concentrations.[13–16] In this context, several studies have reported on the use of advanced electrogravimetry for studying pseudocapacitive materials such as conducting polymers: polypyrrole (PPy),[17] polyaniline (Pani),[18] and Prussian blue (PB);[16] and metal oxides, e.g. ZnO,[19] WO_3,[20] and MnO_2.[21] These works highlighted the advantage of using *ac*-electrogravimetry to explain in details the process occurring at the EEI and its ability to discriminate between cations, anions, and solvent molecules transferred at the electrode surface, and therefore to understand the charge storage properties of the electrode materials. In the case of nanocomposite materials, the electrogravimetric methods have been used not only to explain the combination of the properties of different phases in the nanocomposite, but also to reveal the creation of other active sites for the ions exchange.[22–24] For example, the CNT/PB

nanocomposite has been characterized by EQCM and *ac*-electrogravimetric methods in order to underline the benefit of this combined method on the charge storage properties. Indeed, a synergistic interaction between the two phases was identified and different sites in the nanocomposite were accessible for both electroadsorption/insertion of the different species.[22]

Poly *ortho*-phenylenediamine (P*o*PD) has shown an excellent cycling stability as electrode for supercapacitors and a great promise for developing P*o*PD-based nanocomposite with carbon nanomaterials,[25] which could provide enhanced properties for energy storage devices. For instance, Sacer *et al*.[26] have studied the electroactivity of GO/P*o*PD composite by EQCM. The results showed an improvement of the electrochemical properties of the composite compared to the P*o*PD alone. Besides, the hydration of the composite film was identified as a rate-limiting process and played an important role for better reversibility of the redox reaction. However, further information about the participation of the charged species during the electrochemical process have not been reported. Another promising structure of P*o*PD-based nanocomposite, combining P*o*PD with CNT, drew attention in the electroanalytical chemistry, electrocatalysis and corrosion fields.[27–31] Besides, as it was reported in our pervious paper, CNT/P*o*PD composite showed enhanced charge storage performance, which was ascribed to the positive synergistic effect between the CNTs and P*o*PD, permitting the electrolyte ions to easily access into the electrode.[32] In contrast, the charge storage mechanisms of CNTs/P*o*PD nanocomposite have not yet been studied in sufficient detail, and the positive synergistic interaction between the two compounds and the access of electrolyte ions into the electrode are not clearly understood.

In this work, we report for the first time a detailed characterization of the charge storage mechanism of CNT/P*o*PD nanocomposite-based electrode using a coupled electrochemical and gravimetric method under dynamic regime. The P*o*PD was prepared on CNT modified electrode by electropolymerization method in acidic medium. Thereafter, the classical EQCM

technique was used to follow the mass variations during the electrochemical cycling of CNT/P*o*PD nanocomposite which presented a non-monotonous dependence as a function of applied potential and its scan rate. Subsequently, *ac*-electrogravimetry was applied in order to discriminate and identify the involvement of different charged and non-charged species. Specifically, access to the kinetic parameters of each species at the EEI was enabled and their relative concentration variation in the electrode was estimated.

2. EXPERIMENTAL

2.1. Prepartion of CNT/P*o*PD nanocomposite

Thin layers made of carbon nanotubes (SWCNT with a diameter of about 0.7-1.1 nm and a length between 300 and 2300 nm, Sigma Aldrich) have been coated on the gold electrode of the quartz crystals (resonant frequency of 9 MHz-AWS form Valencia, Spain) by using drop casting. A 0.9 mg portion of carbon nanotubes and 0.1 mg of poly(vinylidene fluoride-hexafluoropropylene (PVDF-HFP) were dispersed in 5 ml of N-methyl-2-pyrrolidonne (NMP) by ultrasonic treatment to obtain a homogeneous dispersion. A 10 µl of the resulting dispersion was deposited on the gold surface (0.2 cm^2) of quartz crystal electrode by drop-casting using a precise micro-pipette and dried in an oven for 2 h at 120 °C.[13] Thereafter, P*o*PD was formed on CNT modified electrode by electrochemical deposition using a 3-electrode cell, in which, CNT modified electrode, platinum grid, and Ag/AgCl (3 M KCl solution saturated with AgCl; from Sigma-Aldrich) were used as working, counter, and reference electrodes, respectively. The electrodeposition of P*o*PD was performed in 0.1 M sulfuric acid solution containing 5 mM *o*PD (1,2-diaminobenzene monomer, from Sigma-Aldrich) using cyclic voltammetry in the potential range from -0.35 to 0.8 V *vs.* Ag/AgCl at a scan rate of 0.005 $V.s^{-1}$. The difference of the resonant frequency of the quartz crystal (Δf) measured before and after the deposition of CNT and P*o*PD, was used to estimate the mass of CNT/P*o*PD nanocomposite, that is found to be

wt.% ratio of 1/5, according to the Sauerbrey equation ($\Delta f_m = -k_s.\Delta m$) where k_s=16.31 Hz.g^{-1}.cm^2 is the experimental sensitivity coefficient.[33,34] Under our experimental conditions, these films can be considered acoustically thin enough, which keep the gravimetric regime of the QCM device.

2.2. Morphological characterization

The morphology of the electrode surface and the thickness of the film were characterized by a field emission gun scanning electron microscope (FEG-SEM, Zeiss, Supra 55). The chemical composition of the nanocomposite was investigated using an energy dispersive X-ray detector (EDX) coupled to FEG-SEM instrument.

2.3. Electrogravimetric measurements

The electrogravimetric properties of CNT/P*o*PD electrode were investigated using three-electrode configuration in 0.5 M aqueous NaCl solution at pH=2 (pH was adjusted by the addition of HCl). A CNT/P*o*PD coated quartz crystal substrate was used as working electrode, a platinum grid as counter electrode, and Ag/AgCl (3 M KCl solution saturated with AgCl; from Sigma-Aldrich) as reference electrode. Electrochemical quartz crystal microbalance (lab-made QCM device coupled with an Autolab PGSTAT100, potentiostat-galvanostat) measurements were carried out in the potential range from -0.5 V to 0.5 V *vs.* Ag/AgCl at different scan rates.

The *ac*-electrogravimetric measurements, using a lab-made potentiostat (SOTELEM-PGSTAT) were performed at fixed potentials, in the frequency range from 63 kHz to 10 mHz with a small amplitude potential perturbation. The QCM was used under dynamic regime. The *ac* response, ΔI, and the mass change, Δm, were measured simultaneously at given potentials, and the obtained results were analyzed by a four-channel frequency analyser (FRA, Solartron

1254). Thereafter, the electrochemical impedance ($\frac{\Delta E}{\Delta I}(\omega)$), the charge/potential ($\frac{\Delta q}{\Delta E}(\omega)$), and the electrogravimetric ($\frac{\Delta m}{\Delta E}(\omega)$) transfer functions (TFs), were fitted by the theoretical expressions given in **Equations 1-3**, respectively. It should be noted that all the transfer functions, including cross and partial TFs, were fitted with the same parameters (M_i, K_i and G_i: molar mass, kinetics of transfer and inverse of the transfer resistance, respectively), and good agreement of both shape and frequency between the experimental and the theoretical curves were obtained (see Refs. [16,17,35–37] for more details).

3. RESULTS AND DISCUSSION

3.1. Preparation and characterization of CNT/P*o*PD nanocomposites

The electropolymerization of *o*PD (on bare gold-patterned quartz substrate and on CNT modified electrode) by cyclic voltammetry were performed, as described previously (**Fig. S1**). During the 1st cycle, both electrodes show a peak of the monomer oxidation at 0.6 V with a current density of about 2 mA cm^{-2} (**Fig. S1a**). After several cycles, two redox peaks appeared at around -0.2 V (for the 1st redox peak) and around 0 V (for the 2nd redox peak) as shown in **Fig. S1b**. In the subsequent cycles, the current value of these redox peaks increases, while that of the oxidation peak of the monomer decreases, indicating that polymerization of *o*PD is successful and the P*o*PD film grows on the surface of the electrodes. After 200 CV cycles, the polymerization of *o*PD on CNT shows a higher current density compared to the polymerization on bare gold electrode (**Fig. S1b**). This behavior is principally attributed to the high surface area of the CNT coating, resulting in improved electrical properties of the nanocomposite.[38,39] The obtained result is in agreement with the earlier reports.[40,41] Then, the resulting films were characterized using FEG-SEM coupled to EDX detector. **Fig. 1 and Fig. S2** show the FEG-SEM images of CNT, PoPD, and CNT/PoPD nanocomposite coated quartz crystal substates.

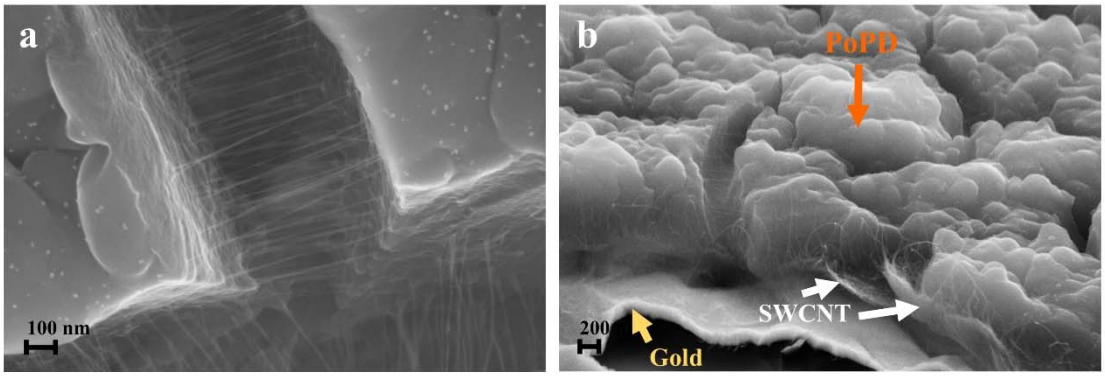

Figure 1. FEG-SEM images of CNT/PoPD nanocomposite deposited on gold-patterned quartz electrodes.

Fig. S2a shows the surface morphology of the film denoted as CNT thin film, displaying a network composed of bundles of single wall CNT with an average size of about 10-20 nm, as described previously.[35] The FEG-SEM image of P*o*PD film (**Fig. S2b**) shows a nodular structure on the surface which extends to a compact film with an average thickness of about 150 nm. In the **Fig. 1a** and **Fig. 1b**, the CNT/P*o*PD nanocomposite film images show a part of the CNT network integrated in the P*o*PD film. This morphology is expected to provide a high mechanical robustness and continuous pathways for electron transport. As it is observed in the cross-section image (**Fig. 1b**), the nanocomposite film has an average thickness of about 700 nm. The association of the two components gives the possibility to benefit from both EDLC behavior of CNTs and faradic reaction of P*o*PD. The CNT/P*o*PD nanocomposite were also analyzed by EDX detector coupled to FEG-SEM in order to determine the chemical composition. As shown in **Fig. S3**, the intense C peak in the EDX spectrum indicates the presence of C related to the CNT and P*o*PD. The presence of N and O confirm the formation of P*o*PD on the CNT film. In addition, the spectrum shows the presence of Au and Si of the gold-patterned quartz electrode.

3.2. Interface analyses by electrochemical quartz crystal microbalance

The electrochemical behavior of CNT/P*o*PD nanocomposite film was characterized using CV coupled to the quartz crystal microbalance in aqueous 0.5 M NaCl solution at different scan rates (**Fig. 2**). **Fig. 2a** shows the typical redox behavior of P*o*PD.[25] The peak-to peak separation increase with the increase of scan rate from 10 to 100 $mV.s^{-1}$, indicating a limitation in the charge transfer process.[42,43] The simultaneous mass changes were also reported as function of potential and at different scan rates (**Fig. 2b**).

Considering the curve of 10 $mV.s^{-1}$, a particular behavior is observed: during the reduction, the mass decreases from 0.5 V to 0.1 V, followed by an increase in the mass from 0.1 V to -0.4 V, and at the end, the mass decreases from -0.4 V to -0.5 V. With an initial evaluation of this behavior at the cathodic scan, the decrease of the mass can be attributed to a major contribution of anions, whereas the increase of the mass can be related to a main response of cations. The higher scan rates lead to a major change in the Δmass profiles, especially evident

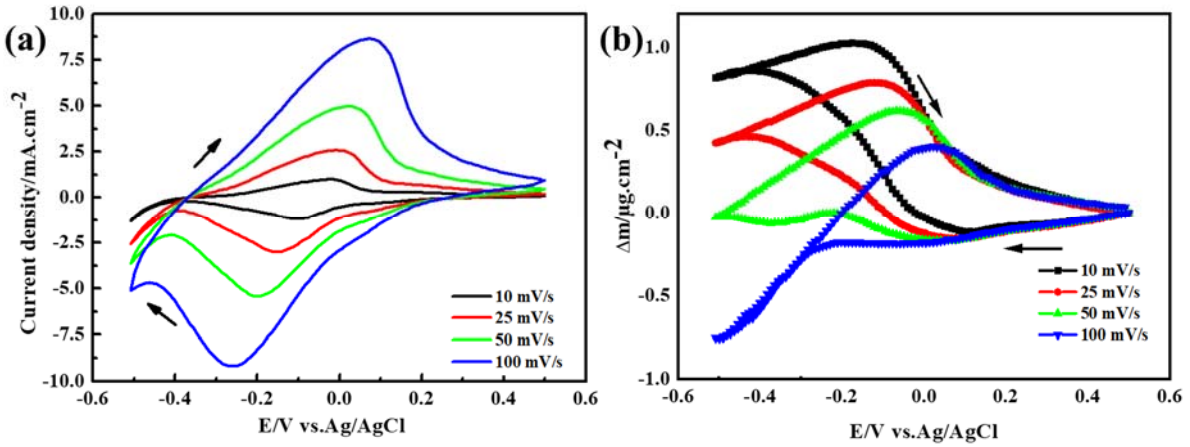

Figure 2. (a) CV curves, and (b) mass responses of the CNT/P*o*PD nanocomposite in 0.5 M NaCl at pH=2, from -0.5 to 0.5 V, with different scan rates.

in the potential range between 0.1 V to -0.5 V. The mass response observed at more cathodic potentials may corresponds to an anion and/or a non-charged species contribution (with opposite flux direction to cations), which gradually increases from 10 $mV.s^{-1}$ to 100 $mV.s^{-1}$ and starts to dominate the global mass response. This result can be related to the transfer of several

species with different portions and kinetics. In order to elucidate this phenomenon, already revealed by the EQCM data, the *ac*-electrogravimetry was performed at different fixed potentials in the range from -0.4 to 0.4 V *vs.* Ag/AgCl. The latter complementary method has been shown to be beneficial to study the interfacial charge transfer mechanisms. Accordingly, using these analyses, we expect (i) to identify the nature and the transfer kinetics of different species that contribute into interfacial charge compensation occurring in CNT/P*o*PD nanocomposite films and (ii) to explain the scan-rate dependent atypical mass change observed in the EQCM results.

3.3. Interface analyses by electrogravimetric impedance spectroscopy (*ac*-electrogravimetry)

3.3.1. Identification of the involved species in the charge storage mechanism of CNT/P*o*PD

Ac-electrogravimetric measurements were performed in aqueous NaCl solution at different fixed-potentials from -0.4 to 0.4 V *vs.* Ag/AgCl with a potential perturbation amplitude of 50 mV. The experimental electrochemical impedance, $\frac{\Delta E}{\Delta I}(\omega)$, the charge/potential, $\frac{\Delta q}{\Delta E}(\omega)$, and the mass/potential, $\frac{\Delta m}{\Delta E}(\omega)$ transfer functions (TF), were obtained from *ac*-electrogravimetry. The charge/potential TF can determine the interfacial transfer of ionic species, while the mass/potential TF discriminates the nature of different charged species (anions, cations), as well as the free solvent contributions.[16,17]

Fig. 3 shows the results of the electrochemical impedance, the charge/potential, and mass/potential TFs of CNT/P*o*PD nanocomposite measured at 0 V *vs*. Ag/AgCl. **Fig. 3a** presents the electrochemical impedance, which shows a slightly inclined straight line at low frequencies, indicating the contribution of multi-ions into the charge compensation process. The charge/potential transfer function (**Fig. 3b**) exhibits one suppressed loop which can be

attributed to the participation of more than one charged species. The difference in the time constant of the species is not sufficient to permit them to be seen as separate loops. Characteristic frequencies range from 10 Hz to 0.01 Hz.

The experimental data of electrochemical impedance and charge/potential TF were fitted using the following theoretical expressions:

$$\frac{\Delta E}{\Delta I}(\omega) = (j\omega d_f F \sum_i \frac{G_i}{j\omega d_f + K_i})^{-1} \quad \text{(i: ions)} \qquad \textbf{(Equation 1)}$$

$$\frac{\Delta q}{\Delta E}(\omega) = F d_f \sum_i \frac{G_i}{j\omega d_f + K_i} \quad \text{(i: ions)} \qquad \textbf{(Equation 2)}$$

where K_i describes the kinetics of species' transfer, G_i represents the ease/difficulty of each species' transfer at the electrode/electrolyte interface, d_f is the film thickness and F is Faraday constant. The obtained curves of the experimental data and the theoretical fit show a successful agreement, revealing the contribution of three charged species. The fitting process provides the values of K_i and G_i parameters of each species, which are reported in **Table S1**. However, the results obtained by electrochemical impedance and charge/potential TF do not allow the identification of nature of these species to be clarified. Therefore, the mass/transfer function was used to identify all the species (charged and neutral), to follow their flux direction and to estimate their kinetics of transfer.

The obtained parameters (K_i and G_i) of the charged species (from **Equation 1** and **2**) are used in the fitting of the mass/potential TF according to the following equation:

$$\frac{\Delta m}{\Delta E}(\omega) = -d_f \sum_i M_i \frac{G_i}{j\omega d_f + K_i} \quad \text{(i: ions and neutral species)} \qquad \textbf{(Equation 3)}$$

where M_i is the molar mass of the species involved in the charge compensation mechanism. The additional parameter appears in the theoretical mass/potential TF (**Equation 3**), *i.e.* the

molar mass (M_i) of each species, is used to identify the nature of the ionic or non-ionic species contributing to the charge compensation mechanism.

Fig. 3c presents the experimental and the theoretical curves corresponding to the mass/potential TF for CNT/P*o*PD nanocomposite film. The curve shows two well defined loops emerged in different quadrants. From a theoretical standpoint, the contributions of anionic species appear in the first (I) and the fourth (IV) quadrant, and the contributions of cations appear in the second (II) and third (III) quadrant, depending on their interfacial transfer kinetics.[16,17] However, the transfer of free solvent molecules depends of their flux, and thus, they can be detected in the same quadrant either with anions or cations.[44]

The fitting of the experimental $\frac{\Delta m}{\Delta E}(\omega)$ data using the theoretical expression (**Equation 3**) and with the parameters given in **Table S1** reveals the participation of three charged species Cl^-, Na^+, H^+ and free H_2O molecules at intermediate frequencies. It is noted that the mass/potential TF (**Equation 3**) involves the M_i (the molar mass of the species involved in the charge compensation mechanism), which enables the identification of the species, thus differentiating between H^+ from H_3O^+ and bare Na^+ from hydrated sodium species. The experimental and theoretical curves showed a good agreement (**Fig. 3c**).

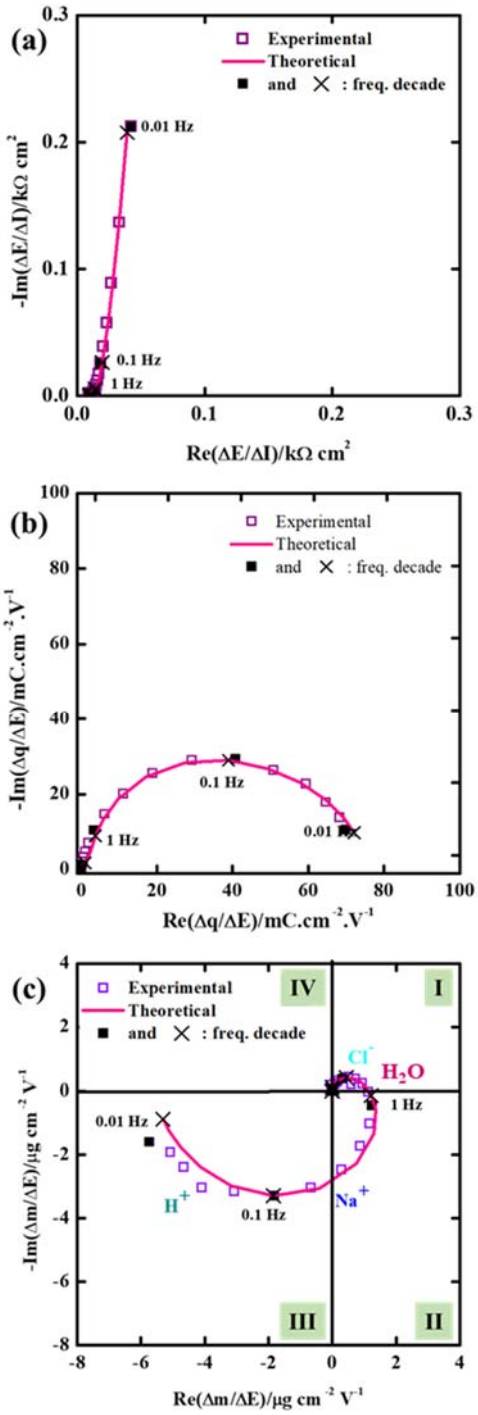

Figure 3. Experimental and theoretical of (a) electrochemical impedance, $\frac{\Delta E}{\Delta I}(\omega)$, (b) charge/potential, $\frac{\Delta q}{\Delta E}(\omega)$, and (c) mass/potential, $\frac{\Delta m}{\Delta E}(\omega)$, transfer functions of the CNT/P*o*PD film measured at 0 V vs. Ag/AgCl in 0.5 M NaCl solution at pH=2.

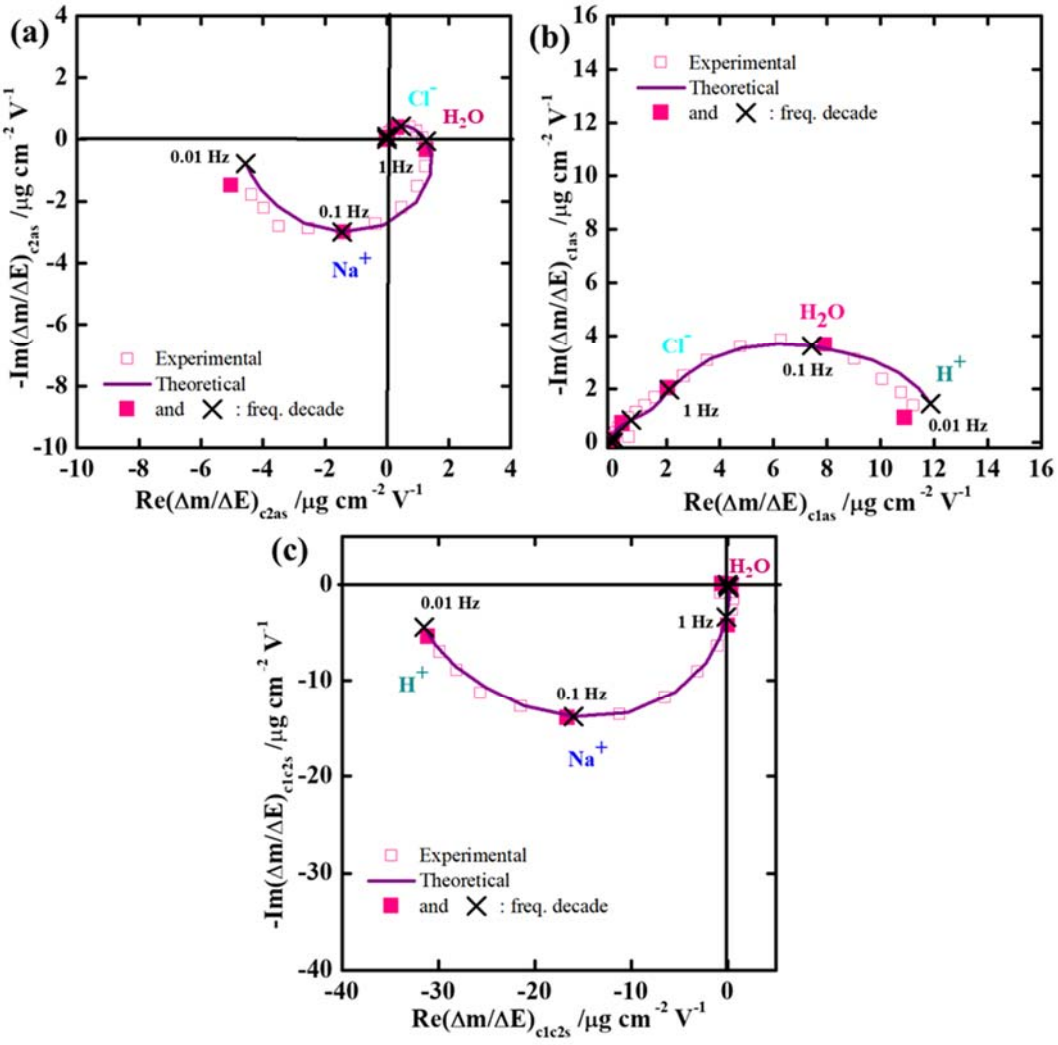

Figure 4. Partial *ac*-electrogravimetric data shown 0 V *vs.* Ag/AgCl. $\frac{\Delta m}{\Delta E}\Big|^{c2as}$ (ω) TF **(a)**; $\frac{\Delta m}{\Delta E}\Big|^{c1as}$ (ω) TF **(b)** and $\frac{\Delta m}{\Delta E}\Big|^{c1c2s}$ (ω) TF **(c)** of CNT/PoPD film measured in 0.5M NaCl solution at pH=2.

Escobar-Teran *et al.*[35] have studied the electrogravimetric behavior of SWCNT under the same conditions of our study. The results show that the response of SWCNT thin film at 0 V *vs.* Ag/AgCl presents the participation of only charged species (Cl^-) and free solvent (H_2O). While, the electrogravimetric response of P*o*PD polymer film shows no species involvement at the same potential.[25] Accordingly, the pairing the CNT and the P*o*PD polymer exhibits a positive synergetic effect, which leads to the creation of other active sites for the ion exchange.

In order to further confirm the participation of the four different species identified in the **Fig. 3c**, the partial electrogravimetric transfer functions have been reported in **Fig. 4**. These functions are calculated by removing the contribution of one of the species and checking the quality of the fit of the remaining contribution, which provides a validation/control procedure of the proposed model. As shown in **Fig. 4**, the resulting curves of the experimental data and the theoretical fit showed a successful agreement, which confirm our hypothesis about the nature, kinetic and contribution of different identified species.

3.3.2. Transfer dynamics of different species involved in the charge storage mechanism of CNT/P*o*PD film

In **Fig. 3** and **Fig. 4**, *ac*-electrogravimetric results at 0 V *vs*. Ag/AgCl were reported. It should be noted that the *ac*-electrogravimetric analyses were performed at several potentials in the range from -0.4 to 0.4 V *vs.* Ag/AgCl. From the *ac*-electrogravimetric measurements, the characteristic frequencies, f_i, associated to the kinetics and the resistance of transfer of each species, Rt_i, can be determined. By using K_i and G_i parameters of each transferred species, f_i and Rt_i were calculated using the following formula: $f_i = \frac{K_i}{\pi d_f}$ and $Rt_i = \frac{1}{\mathrm{F}G_i}$, respectively.

The calculated values of f_i and Rt_i were reported in **Table S1**. **Fig. 5a** and **Fig.5b** present the variation of f_i and Rt_i of each species at different potential in the potential range studied. The results show that the order of the transfer kinetics at different potentials presents the following tendency: f_i (Cl^-) > f_i (H_2O) > f_i (Na^+)> f_i (H^+). In contrast, the transfer resistance of the species, Rt_i, showed an inverse behavior to their transfer kinetics.

The *ac*-electrogravimetry reveals the contribution of multi-species with different kinetics and resistance of transfer. These results confirm the hypothesis discussed previously to explain the change in the mass variation curves as a function of the scan rate reported in **Fig. 2b**. As shown

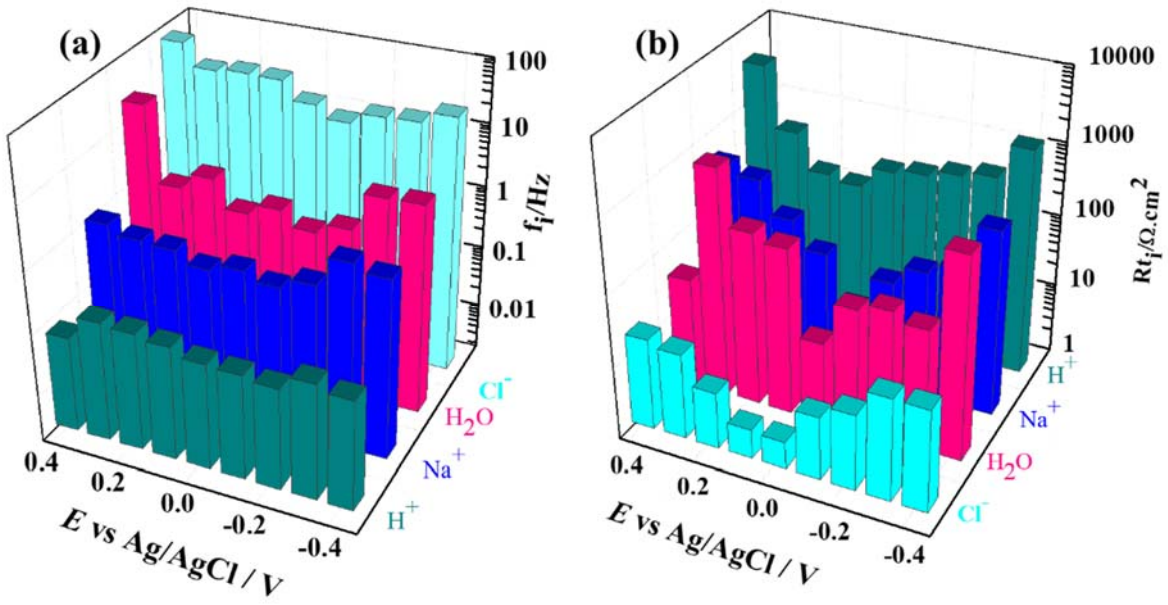

Figure 5. Variation of (a) the characteristic frequency (f_i) and (b) the transfer resistance (Rt_i) of the CNT/P*o*PD film measured in 0.5 M NaCl solution at pH=2.

in **Fig. 2b**, at 100 mV.s^{-1}, the electrochemical behavior of CNT/P*o*PD nanocomposite during the oxidation shows a large mass increase followed by a mass decrease. It is important to highlight that this EQCM profile described with the participation of anions became more pronounced at high scan rates. Indeed, the anion contribution is detected at high frequency (faster process) in the *ac*-electrogravimetric measurements which strengthens the idea that anion contribution is amplified for the high values of the scan rates in the EQCM (**Fig. 2**). While at lower scan rate (from 50 to 10 mV.s^{-1}), the behavior observed at 100 mV.s^{-1} gradually becomes less evident and the mass response (**Fig. 2b**) in EQCM becomes dominated by the cation contribution. It means that the cation contribution, as it exhibits at a slow transfer process, is hardly detected at high scan rate, but starts to govern the electrogravimetric response at lower scan rates.

At more anodic potentials (from 0 V to 0.4 V *vs*. Ag/AgCl), the CNT/P*o*PD nanocomposite shows the contribution of Cl^- and H_2O, which can be caused by the presence of SWCNT.[35]

Indeed, the P*o*PD alone does not show any gravimetric response at these potentials as depicted in our former study.[25] But the contributions of Na^+ and H^+, seen in the case of the CNT/P*o*PD nanocomposite, have not been detected neither in the CNT nor in the P*o*PD films, in the above mentioned potential range. This effect can be related to a synergetic effect between CNT and P*o*PD, which creates other active sites in the nanocomposite structure.

3.3.3 Gravimetric contribution of each species in the charge storage mechanism of CNT/P*o*PD film; correlation between *ac*-electrogravimetric and EQCM results

The estimation of the relative concentration of each species, C_i, with respect to the potential variation is one of the assets of the *ac*-electrogravimetry. This can be achieved using the **Equation 5**, which is obtained through an integration process of the **Equation 4**:

$$\frac{\Delta C_i}{\Delta E}(\omega) = \frac{-G_i}{j\omega d_f + K_i} \qquad \textbf{(Equation 4)}$$

$$C_i - C_0 = \int_{E_0}^{E_i} \frac{\Delta C_i}{\Delta E}(\omega)\,dE\Big|_{\omega\to 0} = \int_{E_0}^{E_i} \frac{-G_i}{K_i}\,dE \qquad \textbf{(Equation 5)}$$

Fig. 6a presents the relative concentration changes ($C_i - C_0$) of individual species identified by *ac*-electrogravimetry. The $C_i - C_0$ evolution of Na^+ and H^+ are higher that the $C_i - C_0$ changes of Cl^- and H_2O, especially at cathodic potentials. It is important to note that in spite of the lower kinetics of transfer, protons present a non-negligible contribution. Their participation to the charge compensation mechanism of P*o*PD was described as a proton addition-elimination reaction, due to the motion of electrolyte ions together with electron transfer.[43] In comparison with the gravimetric response of SWCNT[35] and of P*o*PD[25] under the same conditions, the CNT/P*o*PD nanocomposite presents collective effects caused by the redox process of P*o*PD and the electroadsorption process on CNT, in addition to enhancing the accessibility to the new sites for ion exchange.

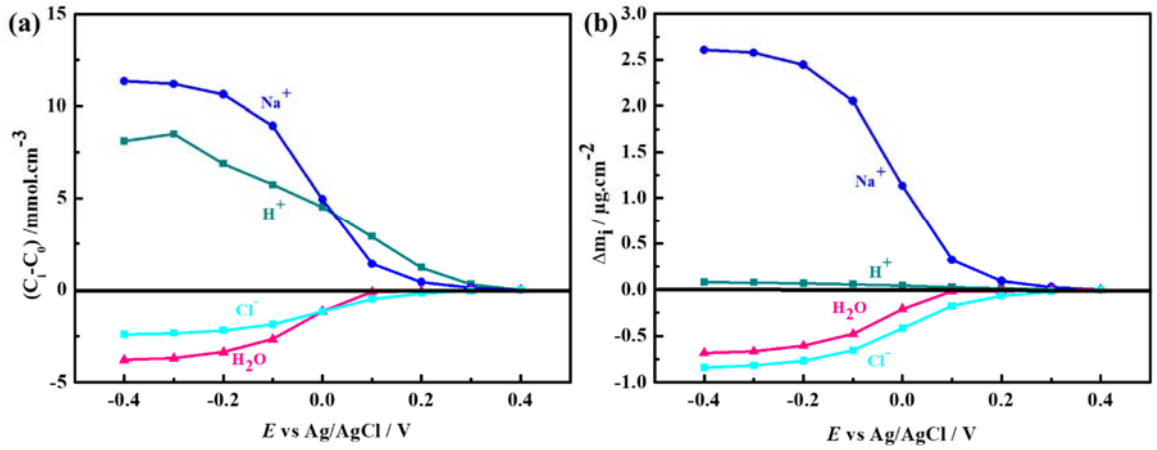

Figure 6. *Ac*-electrogravimetric results of the CNT/PoPD film deposited on gold-patterned quartz crystal electrode. (a) Variation of the relative concentration (C_i – C_0) and (b) the corresponding relative mass variation of each species, Δm_i, calculated at different potentials.

The relative mass variations of each species at different potentials were calculated (**Fig. 6b**), using the relative concentration changes presented in **Fig. 6a**. The gravimetric contributions of the different species implicated in the electrochemical process present a different behavior, Na^+ mainly dominates the Δm response, while the H^+ has not a significant effect due to its low atomic mass. The gravimetric reconstruction of the global mass variation can be calculated by the addition of different mass contributions presented in **Fig. 6b** and compared with that of classical EQCM (**Fig. 7a** and **Fig.7b**). The global mass variation ($\Delta m_{ac\text{-electrogravimetry}}$: obtained from *ac*-electrogravimetry results at different potentials) (**Fig. 7b**), shows a good agreement with the mass variation at the low scan rate (10 $mV.s^{-1}$) measured with the classical EQCM (**Fig. 7a**). This comparative study further confirms the contribution of different species detected by *ac*-electrogravimetry and emphasizes the complementarity of the latter to the classical EQCM.

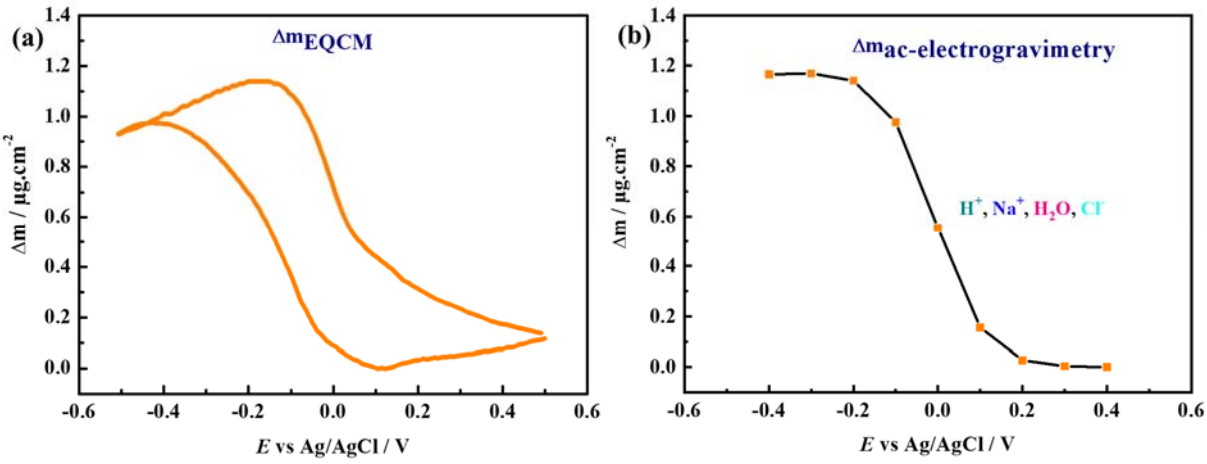

Figure 7. Mass variation (a) obtained by EQCM at 10 $mV.s^{-1}$ and (b) reconstructed from *ac*-electrogravimetry. Measurements were performed in the same conditions.

4. CONCLUSIONS

We have reported on the electrochemical charge storage mechnisms of CNT/P*o*PD nanocomposite in aqueous media, thorough investigation of the results obtained *via in situ* advanced electrogravimetric methods. After the successful formation of CNT/P*o*PD by the electropolymerization of *o*PD on CNT modified gold-patterned quartz electrode, EQCM analyses in acidic NaCl media revealed that the charge transfer process of the nanocomposite modified electrodes takes place with the participation of multi-species. Thereafter, *ac*-electrogravimetry measurements were performed to better understand the global EQCM response and to investigate the transfer dynamics of each species exchanged at the CNT/P*o*PD electrode surface. It was found that the Cl^- contribution is detected at high frequencies, due to its fast process, followed by H_2O molecules in the same flux direction as Cl^-. While, at lower frequencies, Na^+ and H^+ were involved through slower process in the opposite flux direction to Cl^- and H_2O. Regarding their gravimetric contribution, the relative concentration of Na^+ and H^+ were higher than that of Cl^- and H_2O. Besides, Na^+ mainly dominated the Δm response of the

composite electrode, while H^+ did not have a significant effect due to its low atomic mass. These finding~~,~~ shed the light on the positive synergistic interaction between CNT and P*o*PD, leading to the enhanced accessibility to new sites for ion ~~exchange~~ transfer in the composite electrode, which have not been detected in ~~niether~~ the pristine CNT and P*o*PD films.

SUPPLEMENTARY MATERIAL

Electrochemical polymerization of oPD, FEG-SEM images of CNT, PoPD and CN/PoPD, EDX analysis of SWCNT/PoPD, and the estimated values for $\boldsymbol{K_i}$, $\boldsymbol{G_i}$, $\boldsymbol{Rt_i}$ and $\boldsymbol{f_i}$ parameters extracted from the fitting results of *ac*-electrogravimetry measurements are provided in the supplementary material.

ACKNOWLEDGEMENTS

The authors thank Mrs Stéphanie Delbrel and Mrs Françoise Pollier for FEG-SEM analysis (LISE, UMR 8235, Sorbonne University, France).

NOTES

The authors declare no conflicts of interests.

The data that support the findings of this study are available from the corresponding author upon reasonable request.

REFERENCES

(1) Song, W.-J.; Lee, S.; Song, G.; Son, H. B.; Han, D.-Y.; Jeong, I.; Bang, Y.; Park, S. Recent Progress in Aqueous Based Flexible Energy Storage Devices. *Energy Storage Mater.* **2020**, *30*, 260–286. https://doi.org/10.1016/j.ensm.2020.05.006.

(2) Li, X.; Chen, X.; Jin, Z.; Li, P.; Xiao, D. Recent Progress in Conductive Polymers for Advanced Fiber-Shaped Electrochemical Energy Storage Devices. *Mater. Chem. Front.* **2021**, *5* (3), 1140–1163. https://doi.org/10.1039/D0QM00745E.

(3) Wu, F.; Liu, M.; Li, Y.; Feng, X.; Zhang, K.; Bai, Y.; Wang, X.; Wu, C. High-Mass-Loading Electrodes for Advanced Secondary Batteries and Supercapacitors. *Electrochem. Energy Rev.* **2021**, *4* (2), 382–446. https://doi.org/10.1007/s41918-020-00093-0.

(4) Simon, P.; Gogotsi, Y. Perspectives for Electrochemical Capacitors and Related Devices. *Nat. Mater.* **2020**, *19* (11), 1151–1163. https://doi.org/10.1038/s41563-020-0747-z.
(5) Shao, H.; Wu, Y.-C.; Lin, Z.; Taberna, P.-L.; Simon, P. Nanoporous Carbon for Electrochemical Capacitive Energy Storage. *Chem. Soc. Rev.* **2020**, *49* (10), 3005–3039. https://doi.org/10.1039/D0CS00059K.
(6) Ma, W.; Li, W.; Li, M.; Mao, Q.; Pan, Z.; Hu, J.; Li, X.; Zhu, M.; Zhang, Y. Unzipped Carbon Nanotube/Graphene Hybrid Fiber with Less "Dead Volume" for Ultrahigh Volumetric Energy Density Supercapacitors. *Adv. Funct. Mater.* **2021**, *31* (19), 2100195. https://doi.org/10.1002/adfm.202100195.
(7) Zhu, S.; Ni, J.; Li, Y. Carbon Nanotube-Based Electrodes for Flexible Supercapacitors. *Nano Res.* **2020**, *13* (7), 1825–1841. https://doi.org/10.1007/s12274-020-2729-5.
(8) Liu, Y. M.; Merlet, C.; Smit, B. Carbons with Regular Pore Geometry Yield Fundamental Insights into Supercapacitor Charge Storage. *ACS Cent. Sci.* **2019**, *5* (11), 1813–1823.
(9) Raymundo-Piñero, E.; Kierzek, K.; Machnikowski, J.; Béguin, F. Relationship between the Nanoporous Texture of Activated Carbons and Their Capacitance Properties in Different Electrolytes. *Carbon* **2006**, *44* (12), 2498–2507.
(10) Chmiola, J.; Yushin, G.; Gogotsi, Y.; Portet, C.; Simon, P.; Taberna, P. L. Anomalous Increase in Carbon Capacitance at Pore Sizes Less Than 1 Nanometer. *Science* **2006**, *313* (5794), 1760–1763.
(11) Ye, J.; Wu, Y.-C.; Xu, K.; Ni, K.; Shu, N.; Taberna, P.-L.; Zhu, Y.; Simon, P. Charge Storage Mechanisms of Single-Layer Graphene in Ionic Liquid. *J. Am. Chem. Soc.* **2019**, *141* (42), 16559–16563.
(12) Barisci, J. N.; Wallace, G. G.; Baughman, R. H. Electrochemical Quartz Crystal Microbalance Studies of Single-Wall Carbon Nanotubes in Aqueous and Non-Aqueous Solutions. *Electrochimica Acta* **2000**, *46* (4), 509–517.
(13) Escobar-Teran, F.; Arnau, A.; Garcia, J. V.; Jiménez, Y.; Perrot, H.; Sel, O. Gravimetric and Dynamic Deconvolution of Global EQCM Response of Carbon Nanotube Based Electrodes by Ac-Electrogravimetry. *Electrochem. Commun.* **2016**, *70*, 73–77.
(14) Bourkane, S.; Gabrielli, C.; Keddam, M. Kinetic Study of Electrode Processes by Ac Quartz Electrogravimetry. *J. Electroanal. Chem. Interfacial Electrochem.* **1988**, *256* (2), 471–475.
(15) Lemaire, P.; Sel, O.; Alves Dalla Corte, D.; Iadecola, A.; Perrot, H.; Tarascon, J.-M. Elucidating the Origin of the Electrochemical Capacity in Proton-Based Battery HxIrO4 via Advanced Electrogravimetry. *ACS Appl. Mater. Interfaces* **2019**.
(16) Gabrielli, C.; García-Jareño, J. J.; Keddam, M.; Perrot, H.; Vicente, F. Ac-Electrogravimetry Study of Electroactive Thin Films. I. Application to Prussian Blue. *J. Phys. Chem. B* **2002**, *106* (12), 3182–3191.
(17) Gabrielli, C.; Garcia-Jareño, J. J.; Keddam, M.; Perrot, H.; Vicente, F. Ac-Electrogravimetry Study of Electroactive Thin Films. II. Application to Polypyrrole. *J. Phys. Chem. B* **2002**, *106* (12), 3192–3201.
(18) Torres, R.; Jimenez, Y.; Arnau, A.; Gabrielli, C.; Joiret, S.; Perrot, H.; To, T. K. L.; Wang, X. High Frequency Mass Transfer Responses with Polyaniline Modified Electrodes by Using New Ac-Electrogravimetry Device. *Electrochimica Acta* **2010**, *55* (21), 6308–6312.
(19) Gao, W.; Perrot, H.; Sel, O. Tracking the Interfacial Charge Transfer Behavior of Hydrothermally Synthesized ZnO Nanostructures via Complementary Electrogravimetric Methods. *Phys. Chem. Chem. Phys.* **2018**, *20* (42), 27140–27148.
(20) Razzaghi, F.; Debiemme-Chouvy, C.; Pillier, F.; Perrot, H.; Sel, O. Ion Intercalation Dynamics of Electrosynthesized Mesoporous WO 3 Thin Films Studied by Multi-Scale Coupled Electrogravimetric Methods. *Phys. Chem. Chem. Phys.* **2015**, *17* (22), 14773–14787.
(21) Arias, C. R.; Debiemme-Chouvy, C.; Gabrielli, C.; Laberty-Robert, C.; Pailleret, A.; Perrot, H.; Sel, O. New Insights into Pseudocapacitive Charge-Storage Mechanisms in Li-Birnessite Type MnO2 Monitored by Fast Quartz Crystal Microbalance Methods. *J. Phys. Chem. C* **2014**, *118* (46), 26551–26559.
(22) Escobar-Teran, F.; Perrot, H.; Sel, O. Charge Storage Properties of Single Wall Carbon Nanotubes/Prussian Blue Nanocube Composites Studied by Multi-Scale Coupled Electrogravimetric Methods. *Electrochimica Acta* **2018**, *271*, 297–304.

(23) Gao, W.; Demir□Cakan, R.; Perrot, H.; Sel, O. Electrochemically Reduced Graphene Oxide-Sheltered ZnO Nanostructures Showing Enhanced Electrochemical Performance Revealed by an In Situ Electrogravimetric Study. *Adv. Mater. Interfaces* **2019**, *6* (5), 1801855.
(24) Ressam, I.; Lahcini, M.; Belen Jorge, A.; Perrot, H.; Sel, O. Correlation between the Proton Conductivity and Diffusion Coefficient of Sulfonic Acid Functionalized Chitosan and Nafion Composites via Impedance Spectroscopy Measurements. *Ionics* **2017**, *23* (8), 2221–2227.
(25) Halim, E. M.; Demir-Cakan, R.; Perrot, H.; El Rhazi, M.; Sel, O. Correlation between the Interfacial Ion Dynamics and Charge Storage Properties of Poly(Ortho-Phenylenediamine) Electrodes Exhibiting High Cycling Stability. *J. Power Sources* **2019**, *438*, 227032.
(26) Sačer, D.; Spajić, I.; Kraljić Roković, M.; Mandić, Z. New Insights into Chemical and Electrochemical Functionalization of Graphene Oxide Electrodes by O-Phenylenediamine and Their Potential Applications. *J. Mater. Sci.* **2018**, *53* (21), 15285–15297.
(27) Zhang, X.-H.; Wang, S.-M.; Xu, Z.-X.; Wu, J.; Xin, L. Poly(o-Phenylenediamine)/MWNTs Composite Film as a Hole Conductor in Solid-State Dye-Sensitized Solar Cells. *J. Photochem. Photobiol. Chem.* **2008**, *198* (2), 288–292.
(28) Chen, X.; Zhang, Q.; Qian, C.; Hao, N.; Xu, L.; Yao, C. Electrochemical Aptasensor for Mucin 1 Based on Dual Signal Amplification of Poly(o-Phenylenediamine) Carrier and Functionalized Carbon Nanotubes Tracing Tag. *Biosens. Bioelectron.* **2015**, *64*, 485–492.
(29) Zare, E. N.; Lakouraj, M. M.; Ghasemi, S.; Moosavi, E. Emulsion Polymerization for the Fabrication of Poly(o-Phenylenediamine)@multi-Walled Carbon Nanotubes Nanocomposites: Characterization and Their Application in the Corrosion Protection of 316L SS. *RSC Adv.* **2015**, *5* (84), 68788–68795.
(30) Behzadi, M.; Noroozian, E.; Mirzaei, M. A Novel Coating Based on Carbon Nanotubes/Poly-Ortho-Phenylenediamine Composite for Headspace Solid-Phase Microextraction of Polycyclic Aromatic Hydrocarbons. *Talanta* **2013**, *108*, 66–73.
(31) Gajendran, P.; Saraswathi, R. Enhanced Electrochemical Growth and Redox Characteristics of Poly(o-Phenylenediamine) on a Carbon Nanotube Modified Glassy Carbon Electrode and Its Application in the Electrocatalytic Reduction of Oxygen. *J. Phys. Chem. C* **2007**, *111* (30), 11320–11328.
(32) Halim, E. M.; Demir-Cakan, R.; Debiemme-Chouvy, C.; Perrot, H.; El Rhazi, M.; Sel, O. Poly(*Ortho* -Phenylenediamine) Overlaid Fibrous Carbon Networks Exhibiting a Synergistic Effect for Enhanced Performance in Hybrid Micro Energy Storage Devices. *J. Mater. Chem. A* **2021**, *9* (16), 10487–10496. https://doi.org/10.1039/D1TA00763G.
(33) Sauerbrey, G. Verwendung von Schwingquarzen zur Wägung dünner Schichten und zur Mikrowägung. *Z. Für Phys.* **1959**, *155* (2), 206–222.
(34) Bizet, K.; Gabrielli, C.; Perrot, H. Immunodetection by Quartz Crystal Microbalance. *Appl. Biochem. Biotechnol.* **2000**, *89* (2), 139.
(35) Escobar-Teran, F.; Perrot, H.; Sel, O. Ion Dynamics at the Single Wall Carbon Nanotube Based Composite Electrode/Electrolyte Interface: Influence of the Cation Size and Electrolyte PH. *J. Phys. Chem. C* **2019**, *123* (7), 4262–4273.
(36) Gao, W.; Sel, O.; Perrot, H. Electrochemical and Viscoelastic Evolution of Dodecyl Sulfate-Doped Polypyrrole Films during Electrochemical Cycling. *Electrochimica Acta* **2017**, *233*, 262–273.
(37) Gao, D.; Liu, R.; Yu, W.; Luo, Z.; Liu, C.; Fan, S. Gravity-Induced Self-Charging in Carbon Nanotube/Polymer Supercapacitors. *J. Phys. Chem. C* **2019**, *123* (9), 5249–5254.
(38) Halim, E. M.; Perrot, H.; Sel, O.; Debiemme-Chouvy, C.; Lafdi, K.; El Rhazi, M. Electrosynthesis of Hierarchical Cu2O–Cu(OH)2 Nanodendrites Supported on Carbon Nanofibers/Poly(Para-Phenylenediamine) Nanocomposite as High-Efficiency Catalysts for Methanol Electrooxidation. *Int. J. Hydrog. Energy* **2021**, *46* (38), 19926–19938. https://doi.org/10.1016/j.ijhydene.2021.03.119.
(39) Halim, E. M.; Elbasri, M.; Perrot, H.; Sel, O.; Lafdi, K.; El Rhazi, M. Synthesis of Carbon Nanofibers/Poly(Para-Phenylenediamine)/Nickel Particles Nanocomposite for Enhanced Methanol Electrooxidation. *Int. J. Hydrog. Energy* **2019**, *44* (45), 24534–24545. https://doi.org/10.1016/j.ijhydene.2019.07.141.

(40) Martinusz, K.; Czirók, E.; Inzelt, G. Studies of the Formation and Redox Transformation of Poly(o-Phenylenediamine) Films Using a Quartz Crystal Microbalance. *J. Electroanal. Chem.* **1994**, *379* (1), 437–444.
(41) Zhang, X.-H.; Wang, S.-M.; Wu, J.; Liu, X.-J. Electropolymerization of PoPD from Aqueous Solutions of Sodium Dodecyl Benzene Sulfonate at Conducting Glass Electrode. *J. Appl. Polym. Sci.* **2007**, *104* (3), 1928–1932.
(42) Yadegari, H.; Heli, H.; Jabbari, A. Graphene/Poly(Ortho-Phenylenediamine) Nanocomposite Material for Electrochemical Supercapacitor. *J. Solid State Electrochem.* **2013**, *17* (8), 2203–2212.
(43) Oyama, N.; Ohsaka, T.; Chiba, K.; Takahashi, K. Effects of Supporting Electrolyte and PH on Charge Transport within Electropolymerized Poly(o-Phenylenediamine) Films Deposited on Graphite Electrodes. *Bull. Chem. Soc. Jpn.* **1988**, *61* (4), 1095–1101.
(44) Gao, W.; Debiemme-Chouvy, C.; Lahcini, M.; Perrot, H.; Sel, O. Tuning Charge Storage Properties of Supercapacitive Electrodes Evidenced by In Situ Gravimetric and Viscoelastic Explorations. *Anal. Chem.* **2019**, *91* (4), 2885–2893.

Supplementary material for:

Interfacial charge storage mechanisms of composite electrodes based on poly(*ortho*-phenylenediamine)/carbon nanotubes *via* advanced electrogravimetry

El Mahdi Halim [†,‡], Rezan Demir-Cakan [§,¥], Hubert Perrot [†], Mama El Rhazi [‡], Ozlem Sel [†,]*

[†] Sorbonne Université, CNRS, Laboratoire Interfaces et Systèmes Electrochimiques, LISE, 75005 Paris, France

[‡] University of Hassan II of Casablanca, Faculty of Sciences and Technology, Laboratory of Materials, Membranes and Environment-BP 146, 20650 Mohammedia, Morocco

[§] Institute of Nanotechnology, Gebze Technical University, 41400 Gebze, Kocaeli, Turkey

[¥] Department of Chemical Engineering, Gebze Technical University, 41400 Gebze, Kocaeli, Turkey

***** Corresponding author: ozlem.sel@sorbonne-universite.fr

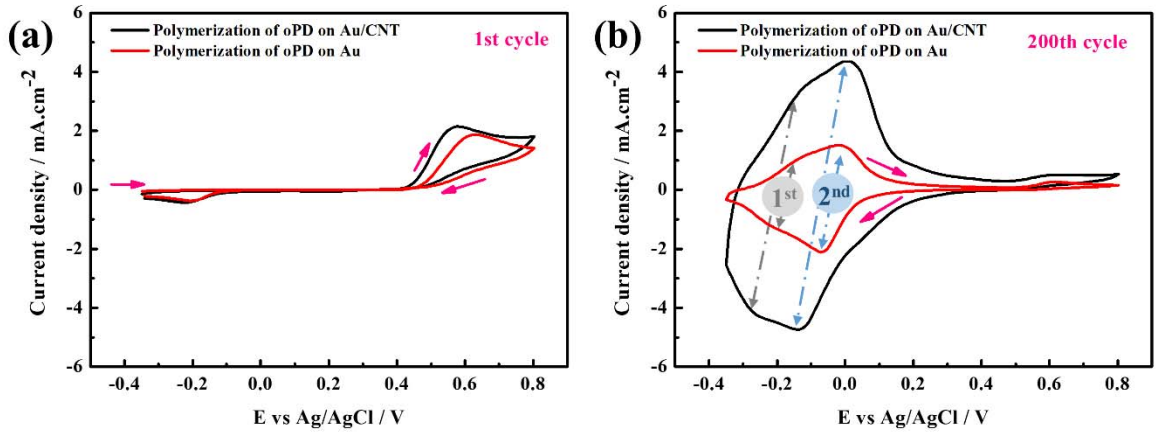

Figure S1. Electrochemical polymerization of oPD on gold-patterned quartz electrode and gold-patterned quartz substrates modified by CNT; a) 1st cycle and b) 200th cycle.

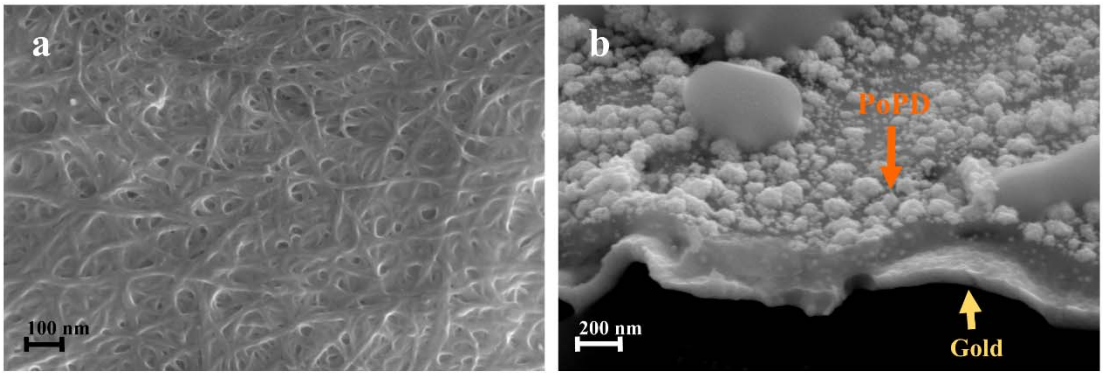

Figure S2. FEG-SEM images of CNT (a) and PoPD (b) deposited on gold-patterned quartz electrodes.

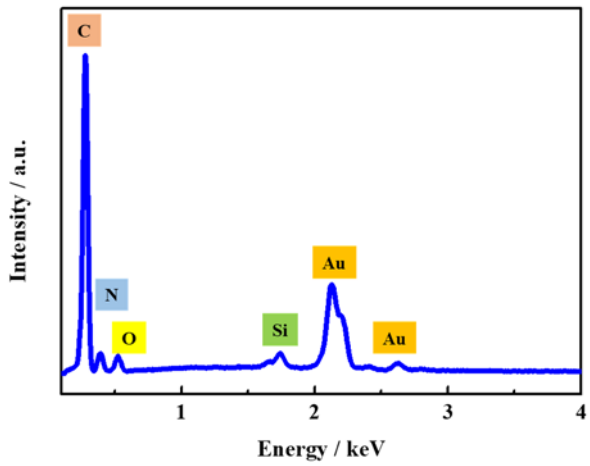

Figure S3. EDX spectrum of SWCNT/PoPD nanocomposite deposited on gold-patterned quartz electrode.

Table S1: Estimated values for K_i, G_i, Rt_i and f_i parameters extracted from the fitting results of *ac*-electrogravimetry measurements of the CNT/PoPD film at 0 V *vs.* Ag/AgCl, measured in 0.5 M NaCl at pH=2. (a: anion, s: solvent, c1: cation1 and c2: cation2)

pH=2	Species identification (***i***)	M_i (g.mol^{-1})	K_i (cm.s^{-1})	G_i (mol.s^{-1}.cm^{-2}.V^{-1})	$Rt_i=1/FG_i$ (Ω.cm^2)	$f_i=K_i/\pi d_f$ (Hz)
at 0 V						
a	Cl^-	35	4.71 10^{-4}	-4.33 10^{-6}	2.39	15.01
s	H_2O	18	3.77 10^{-5}	-7.92 10^{-7}	13.09	1.20
c1	H^+	1	2.83 10^{-6}	3.68 10^{-8}	281.94	0.09
c2	Na^+	23	1.72 10^{-5}	9.50 10^{-7}	10.91	0.55